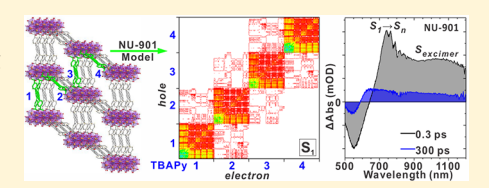


# Excited-State Electronic Properties in Zr-Based Metal—Organic Frameworks as a Function of a Topological Network

Jierui Yu, †, Lo JaeHong Park, Lo Andrea Van Wyk, Garry Rumbles, and Pravas Deria\*, Garry Rumbles, and Pravas Deria\*,

Supporting Information

ABSTRACT: Molecular assemblies in metal-organic frameworks (MOFs) are reminiscent of natural light-harvesting (LH) systems and considered as emerging materials for energy conversion. Such applications require understanding the correlation between their excited-state properties and underlying topological net. Two chemically identical but topologically different tetraphenylpyrene (1,3,6,8tetrakis(p-benzoicacid)pyrene; H<sub>4</sub>TBAPy)-based Zr<sup>IV</sup> MOFs, NU-901 (scu) and NU-1000 (csq), are chosen to computationally and spectroscopically interrogate



the impact of topological difference on their excited-state electronic structures. Time-dependent density functional theorycomputed transition density matrices for selected model compounds reveal that the optically relevant S<sub>1</sub>, S<sub>2</sub>, and S<sub>n</sub> states are delocalized over more than four TBAPy linkers with a maximum exciton size of  $\sim$ 1.7 nm (i.e., two neighboring TBAPy linkers). Computational data further suggests the evolution of polar excitons (hole and electron residing in two different linkers); their oscillator strengths vary with the extent of interchromophoric interaction depending on their topological network. Femtosecond transient absorption (fs-TA) spectroscopic data of NU-901 highlight instantaneous spectral evolution of an intense  $S_1 \rightarrow S_n$ transition at 750 nm, which diminishes with the emergence of a broad (580-1100 nm) induced absorption originating from a fast excimer formation. Although these ultrafast spectroscopic data reveal the first direct spectral observation of fast excimer formation ( $\tau = 2 \text{ ps}$ ) in MOFs, the fs-TA features seen in NU-901 are clearly absent in NU-1000 and the free H<sub>4</sub>TBAPy linker. Furthermore, transient and steady-state fluorescence data collected as a function of solvent dielectrics reveal that the emissive states in both MOF samples are electronically nonpolar; however, low-lying polar excited states may get involved in the excitedstate decay processes in polar solvents. The present work shows that the topological arrangement of the linkers critically controls the excited-state electronic structures.

## ■ INTRODUCTION

Chromophore assemblies, such as those found in natural photosynthetic machinery, have inspired various functional light-harvesting (LH) mimics. As interchromophoric spatial separation can limit screening of their transition dipoles by other electrons,<sup>2</sup> an array of self-assembled chromophores, unlike a single "giant" chromophore, can render composition with high absorptivity.<sup>3</sup> Interchromophoric interactions can potentially generate new pigments with optoelectronic properties<sup>3d</sup> that can tune the exciton lifetime and delocalization and migration lengths that are useful for the various light-harvesting applications. <sup>1f,4</sup> Solar energy harvesting requires a material design strategy that enables the low-lying excited states<sup>5</sup> to drive large exciton displacement and eventually electron-hole pair dissociation.

In this regard, metal-organic frameworks (MOFs)<sup>6</sup> are an emerging class of hybrid optoelectronic materials owing to their enormous design flexibility. These self-assembled molecular compositions are constructed from multitopic chromophore-based linkers densely arranged around pores through coordination bonds, with metal-based nodes generating a vast array of crystalline structures. Structural diversity provides a wide range of pore geometries that make them amenable to dielectric and functional modulation (i.e., installation of secondary chromophores or redox-active species) required for energy harvesting and conversion processes. Frameworks assembled from photoactive building blocks<sup>7a,j,8a-d</sup> can offer unique photophysics and exciton dynamics fundamentally different from those observed in stacked solid chromophore assemblies. While MOF scaffolds provide excellent platforms for exciton hopping and displacement within their chromophoric networks, 7a,b,j,8d they can control interchromophoric interactions engendering modular optoelectronic properties as a function of their spatial orientation. Like other low band gap  $\pi$ -conjugated molecular

Received: May 11, 2018 Published: July 24, 2018

Department of Chemistry and Biochemistry, Southern Illinois University, 1245 Lincoln Drive, Carbondale, Illinois 62901, United States

<sup>\*</sup>Department of Molecular Engineering, Kyoto University, Katsura, Nishikyo-ku, Kyoto 615-8510, Japan

<sup>§</sup>Chemistry and Nanoscience Center, National Renewable Energy Laboratory, Golden, Colorado 80401, United States

Department of Chemistry and Biochemistry and Renewable and Sustainable Energy Institute, University of Colorado at Boulder, Boulder, Colorado 80309, United States

Journal of the American Chemical Society

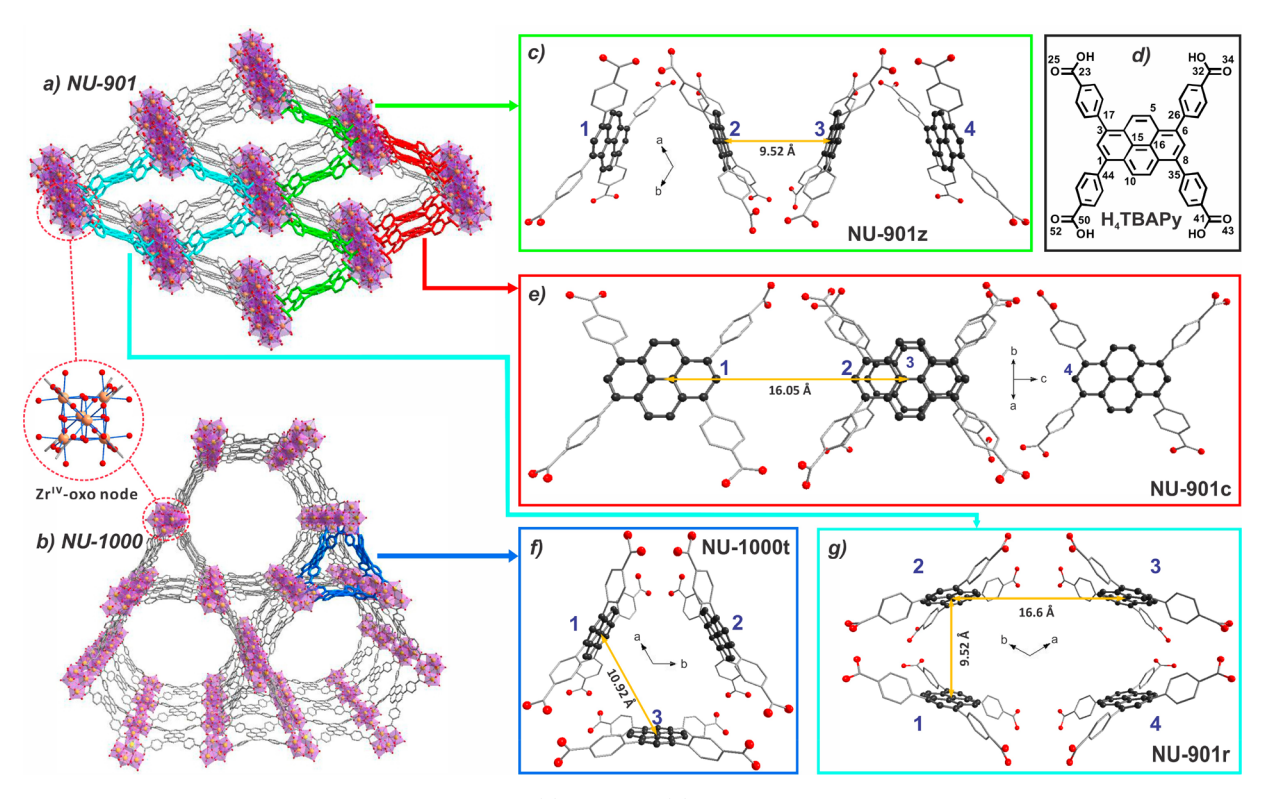


Figure 1. Molecular structures of the TBAPy-based MOFs: (a) NU-901, (b) NU-1000 and their corresponding metal nodes. DFT-optimized structures of various TBAPy cluster models are shown for (c,e,g) NU-901 and (f) NU-1000; the crystallographic origin of the zigzag NU-901z (green), rhombic NU-901r (cyan), crossed NU-901c (red), and triangular NU-1000t (deep blue) models are highlighted in panels (a,b); atom color code: O, red spheres; Zr, golden yellow; C, black spheres or gray sticks; H atoms are omitted for clarity. (d) Chemical structure of the H<sub>4</sub>TBAPy linker with atom numbering scheme used in the time-dependent DFT computations.

LH compositions, 5a-c,10a,b it is expected that a MOF material should feature strong singlet manifold transitions ( $S_0 \rightarrow S_1$ ,  $S_1$  $\rightarrow$  S<sub>0</sub>, and S<sub>1</sub>  $\rightarrow$  S<sub>n</sub>) in the red to the near-infrared (NIR) region to produce delocalized excitons, thereby weakly bound excitons. 11 Thus, it is important to understand the excitonic properties of the optically active singlet excited states (i.e., S<sub>1</sub>,  $S_2$ ,  $S_n$  states) of these crystalline porous chromophore assemblies.

We have recently reported topological control over MOF photophysics<sup>12</sup> in well-established porphyrin-based<sup>12a</sup> and pyrene-based<sup>12b</sup> MOFs featuring the deprotonated form of 5,10,15,20-(tetra-p-carboxyphenyl)porphyrin (H<sub>4</sub>TCPP) or 1,3,6,8-tetrakis(p-benzoicacid)pyrene (H<sub>4</sub>TBAPy) and Zr<sup>IV</sup>based nodes. Zirconium-oxo-based frameworks<sup>13</sup> have recently emerged as a new subclass of MOFs due to their stability stemming from a strong M-carboxylate bond and an "inert" atomic electronic (e.g., diamagnetic) configuration that enable spectroscopic investigations. 7h,12,14a-m Furthermore, their ability to incorporate redox-active species via a postsynthesis functionalization technique 14h,15 makes them attractive for light conversion applications.

Considering their unique spectroscopic properties and topological diversity, we chose two chemically identical TBAPy -ased Zr-MOFs: NU-901  $(scu)^{7h}$  and NU-1000 (csq)(molecular formula  $\operatorname{Zr}_6(\mu_3\text{-O})_4(\mu_3\text{-OH})_4(\text{-OH})_4(\text{-OH})_4$ OH<sub>2</sub>)<sub>4</sub>(TBAPy)<sub>2</sub>; Figure 1) to investigate how topologydependent spatial orientation of the TBAPy linkers impacts the properties of various excited states. Here, we report the electronic structures and excitonic properties in these MOF structures. Transition density matrix (TDM) analyses on various relevant models constructed from a series of small

structural segments provide insight into the excited-state electronic structures that were probed with femtosecond transient absorption (fs-TA) and steady-state and timeresolved emission spectroscopic investigations of the solvent dependence.

## EXPERIMENTAL SECTION

Materials. All spectroscopic grade solvents were purchased from Sigma-Aldrich and used as received. Syntheses of spectroscopic grade MOF samples were reported in our previous publication. 12

Instrumentation. The absorptive electronic transitions for the solid samples were measured as diffused reflectance spectra using a JASCO V-670 UV-vis-NIR spectrophotometer equipped with a 60 mm BaSO<sub>4</sub>-coated integrating sphere. Steady-state emission spectra were recorded using an Edinburgh FS5 spectrofluorimeter. Samples were packed inside a quartz capillary tube (3 mm i.d.) and then sealed and soaked in the respective solvent overnight. These emission spectra were collected in a front-face configuration and corrected using the instrumental correction functions for the excitation light source as well as for the wavelength-dependent detector response. The absolute quantum yields (QY) were measured using a 150 mm integrating sphere and the EI-F980 software that accounts for the diminished intensity counts of the incident beam over the increased intensity counts of fluorescence, based on the manually selected respective integration range. Time-resolved emission decay profiles were recorded using an Edinburgh Lifespec II picosecond timecorrelated single-photon counting spectrophotometer ( $\lambda_{ex} = 405$ nm).12b

Transient absorption spectroscopic data in the femtosecondmicrosecond time domain were collected using either standard pump-probe methods (Ultrafast Systems, HELIOS, Sarasota, FL, USA) or a randomly interleaved pulse train method (picoTAS, Unisoku, Osaka, Japan). The details of the fs-TA spectrometry and the data analysis procedures are described in the Supporting Information (SI). <sup>16</sup> The  $H_4$ TABPy free linker was examined in DMSO solvent (super-dehydrated, Wako Chemical) as a solution. Solid MOF samples (~5 mg/mL) were mixed with inert polystyrene solution (10 mg/mL toluene) and drop-cast on a quartz substrate to ensure transmittance of the probe light with minimal excitation light scattering.

Computational Methods. Electronic excitations and their corresponding energy, oscillator strength, and transition densities were computed for a series of models constructed from various small crystallographic segments (Figure 1) using time-dependent density functional theory (TDDFT//CAM-B3LYP/6-31g(d,p); see Supporting Information for details). Metal-oxo nodes were removed, and a proton was introduced to the carboxylate groups for charge balance; structures were optimized via a constrained DFT. 12,14m Oscillator strengths and their corresponding transition energies were obtained via TDDFT calculations of 60 excited states on these DFT-optimized structures. TDM analyses were performed using the GPview software. 17

## ■ RESULTS AND DISCUSSION

The variable extent of interchromophoric interactions, in different frameworks, leads to unique electronic transitions and excimer formation<sup>12</sup> and should play a crucial role in defining the respective excitonic properties. To understand the extent of interchromophoric interaction among multiple linkers, we first considered a series of model compounds featuring small TBAPy "clusters" that are closely positioned in space within their respective frameworks. Note that these TBAPy cluster models were chosen primarily to facilitate affordable DFT and TDDFT computation on non-exhaustive small systems with the strongest interchromophoric interactions providing electronic properties that can closely represent the spectroscopic signature and excited-state nature of the MOF samples (see SI section B3 for size-dependent properties). These model structures were approximated by replacing the  $\left[ Zr_{6}(\mu_{3} - \mu_{3}) \right]$  $O_4(\mu_3-OH)_4(-OH)_4(-OH)_4$  nodes with protons at each of the carboxylates. This approximation is based on the charge count (i.e., neutral, 8-connected MOF) and the electronic energy levels of the Zr<sup>IV</sup><sub>6</sub>-oxo node that is insignificant in defining the optoelectronic properties of these systems. Recent computational works have established that the electronic energy levels of the wide band gap Zr<sup>IV</sup><sub>6</sub>-oxo nodes (4.5-6.0 eV) lie far relative to the linker frontier orbitals. Thus, the optical properties of the ZrIV6-oxo-based frameworks are defined mainly by linker-centered  $\pi$ - $\pi$ \* transitions. Potentiometric data further establish the unaltered redox potentials of Zr<sup>IV</sup><sub>6</sub>-oxo node-bound TBAPy linkers relative to the H<sub>4</sub>TBAPy benchmark compound due to a type-I alignment of their respective frontier orbitals that do not facilitate significant electronic interactions (see SI section A). Furthermore, the unique electronic energy level alignment between the Zr<sup>IV</sup><sub>6</sub>-oxo node and the  $\pi$ -conjugated linkers is different than that of a Ti<sup>IV</sup>-based system, where the low-lying Ti<sup>IV</sup>-centered lowest unoccupied molecular orbital participates in ligand-to-metal charge transfer (LMCT) or electronic coupling processes. 18b,d Figure 1 highlights a series of such model compounds defining various cofacial and lateral geometries. Combinations of these two different orientations align the TBAPy linkers in an oblique or head-to-tail conformation along the crystallographic a-b and c directions, respectively. The center-to-center distances in these two different interchromophoric conformations are 9.52 Å (between rings 1-2, 2-3, and 3-4 in NU-901z; rings 1-2 and 3-4 in NU-901r; and ring 2-3 in NU-901c), 10.92 Å (between any two rings in NU-1000t), 16.05 Å

(between rings 1-2 and 3-4 in NU-901c), and 16.6 Å (between rings 1-4 and 2-3 in NU-901r).

TDDFT computations on these TBAPy cluster models provide information regarding various excited states. For this, first, the model compounds (Figure 1) were optimized using constrained DFT to maintain the crystallographic coordinates,  $^{12,14\mathrm{m}}$  following which TDDFT computations were performed using the CAM-B3LYP hybrid exchange-correlation functional for the long-range correction using the Coulomb-attenuating method in conjunction with the widely used 6-31g(d,p) basis for C, H, and O atoms. Absorptive transition energies and corresponding oscillator strengths were analyzed for each of these models to examine the evolution of optically active excited states. Figure 2 summarizes the

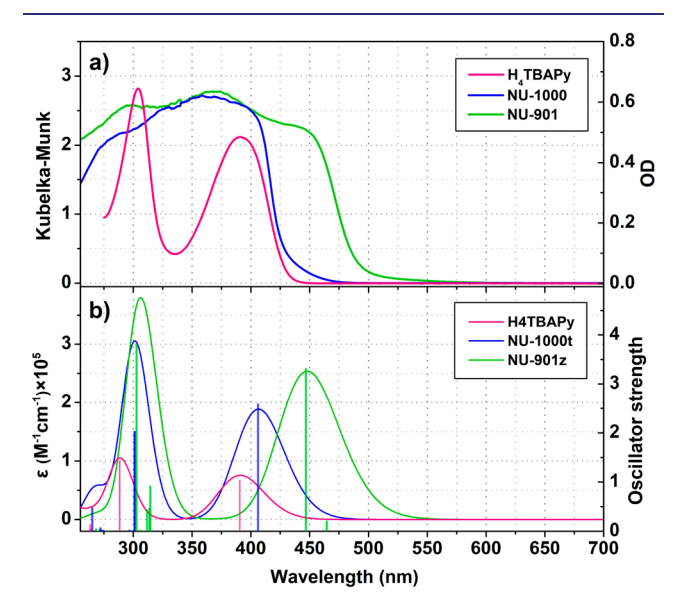


Figure 2. Steady-state electronic absorption spectra: (a) diffuse reflectance spectra of the solid NU-1000 (blue) and NU-901 (green) samples; the pink spectrum represents  $H_4TBAPy$  benchmark in DMF solvent; (b) TDDFT simulated electronic absorptive transitions for the models (Figure 1) and  $H_4TBAPy$  monomer. Note all the simulated spectra (and transition energies) were calibrated against the experimental transition energy of the  $H_4TBAPy$  benchmark compound by 0.303 eV, lowering the computed energy values. The relative difference in the computed oscillator strength, presented in panel (b), is partly due to the number of  $H_4TBAPy$  units present in the corresponding model compounds.

experimental UV-vis absorption spectra for H<sub>4</sub>TBAPy, NU-901, and NU-1000 that clearly highlight the trend predicted by the TDDFT computational data presented in Figure 2b. Note that the simulated spectra and transition energies were calibrated against the experimental H<sub>4</sub>TBAPy benchmark spectra by 0.303 eV lowering the computed data; this energy scaling between the ground and excited states was, at least partially, from nonsolvated systems used for the computation, and this offset does not alter the energy gap between any two excited states. Compared to the H<sub>4</sub>TBAPy benchmark compound, the MOF samples show the lowest energy transitions, significantly red-shifted by ~0.40 eV for NU-901 and a small 0.05 eV for the NU-1000 (Figure 2a). Note that the respective red shifts predicted by TDDFT are 0.42 and 0.03 eV. Figures 3 and S7 summarize the energy of various excited states relative to that of the H<sub>4</sub>TBAPy monomer.

Journal of the American Chemical Society

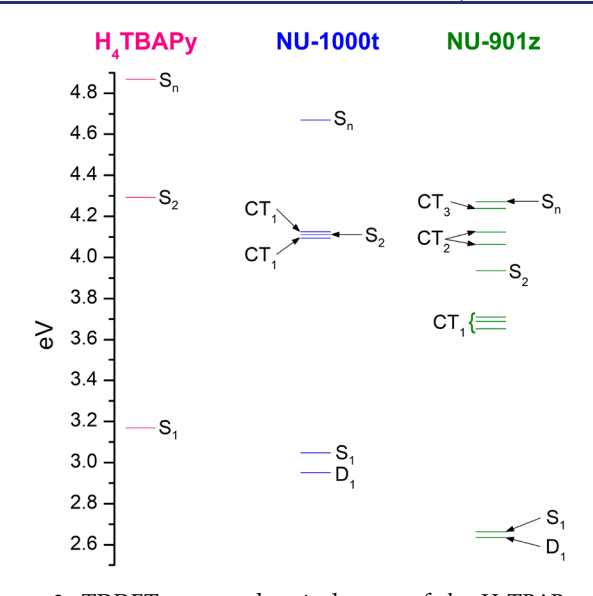
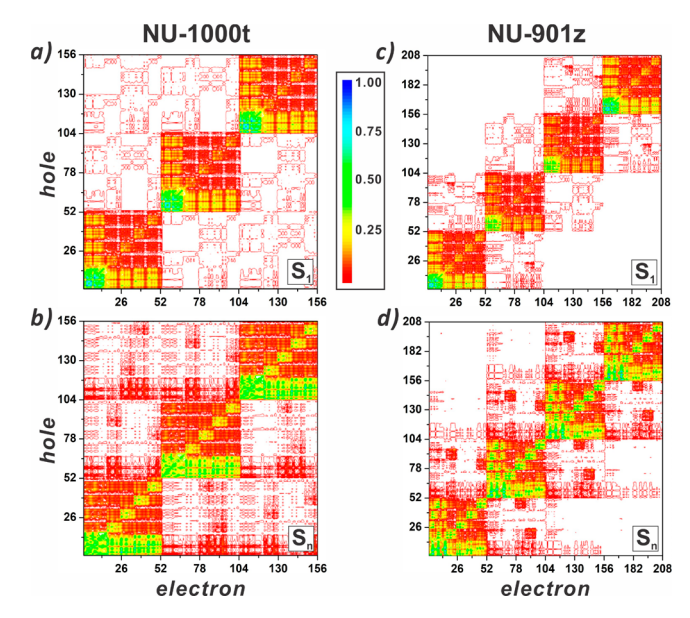


Figure 3. TDDFT computed excited states of the  $H_4$ TBAPy and selected MOF model compounds shown in Figure 1. The energy levels were calibrated against the experimental transition energy of the  $H_4$ TBAPy benchmark compound (i.e., lowering the computed energies by 0.303 eV; Figure 2). Spectroscopically relevant, the lowest energy dark states and the polar (charge-separated) excited states for the MOF model compounds are denoted as  $D_1$  and CT (for NU-901z, the n denotes the number of the TBAPy units for the hole–electron separations; see Figure S5).

Excited-state properties of model compounds were assessed by analyzing TDM. These TDMs represent electronic transitions from the ground state to a given excited state as obtained from the TDDFT computations on the ground-state geometry. The matrix diagonal and off-diagonal densities provide crucial information regarding the distribution of the excitonic wave function (center-of-mass) over the structure and the exciton size (distance between e-h particles), respectively. 20,3c,2 Figure 4 summarizes the representing transitions for NU-1000t and NU-901z (for other model structures, see Figure S8). Excited states were assigned (Figure 3) based on their respective energies, oscillator strengths, and TDM analyses. The diagonal densities for optically allowed S<sub>1</sub> states (Figure 4) indicate that the excitonic wave functions are delocalized over all the TBAPy units. The nonzero off-diagonal densities (e-h distances) for the S<sub>1</sub> states rapidly diminished at the periphery of the linkers (phenyl side arms); nevertheless, the residual density ( $\sim$ 10%) beyond the TBAPy units indicates e-h correlation among the adjacent chromophores with a maximum exciton size of ~1.7 nm. Further examination of the respective S<sub>1</sub> states for various NU-901 models (Figures S7) revealed that NU-901z possesses the lowest energy S1 state originating from the strongest interaction among the TBAPy linkers aligned in oblique geometry. For NU-901r and NU-901c, the TDM plots (Figure S8) indicate that the respective excited states are localized more in the closer cofacial dimers (rings 1-2 and 3-4, Figure 1g; and rings 2-3 in Figure 1e). This observation underscores that the excited states are delocalized more in the direction in which chromophoric linkers are positioned in a cofacial geometry with the shortest center-to-center distance.

In NU-1000, the framework possesses only the triangular motif with cofacial conformation that translates only along the lateral direction of the crystallographic *c*-axis and repeats



**Figure 4.** Contour plot of TDMs corresponding to optically active  $S_1$  and  $S_n$  excited states for model compounds NU-1000t and NU-901z (shown in Figure 2). These plots depict e—h correlation during an optical excitation (i.e., the probability of an electron moving from one molecular position to another). The axes are labeled with atom numbers from each TBAPy unit (shown in Figure 1d).

through the vertices in the a-b plane. In contrast, NU-901 possesses such a cofacial motif that forms an infinite polymeric chain in the a-b plane, which then translates along the c-axis as well as repeats in the a-b plane. For the model compounds, the optically allowed  $S_2$  states have delocalization properties similar to those of the corresponding  $S_1$  states (Figures 4a,c and  $S_0$ ).

The  $S_n$  states play important roles in the photophysical processes within the singlet excitonic manifolds of  $\pi$ -conjugated structures and are usually associated with a strong  $S_1 \rightarrow S_n$  transition dipole moments and a forbidden transition from the ground state. TDM contour plots (Figure 4) of the TDDFT computed excited states for the model compounds (Figure 1) reveal that the  $S_n$  states are delocalized. The significant extent of their off-diagonal densities, relative to their corresponding  $S_1$  state electronic structures, indicate that these are weakly bound nonpolar excitonic states (Figure 4b,d).

Femtosecond transient absorption spectroscopic data of MOF samples (NU-901 and NU-1000), as well as the H<sub>4</sub>TBAPy control sample, unambiguously highlight the impact of MOF topology on the photoinduced products. The fs-TA spectrum of NU-901 at  $t_{\rm delay} = \sim 0.3$  ps upon photoexcitation ( $\lambda_{\rm ex} = 400$  nm; Figure 5a) features an intense induced absorption (IA), centered at around 750 nm that extends beyond 1200 nm as well as a negative spectral signature centered at ~550 nm. Considering the steady-state emission spectrum of NU-901 (Figure S2), we attributed the negative spectral signature to  $S_1 \rightarrow S_0$  stimulated emission and the IA band to the excited-state absorption (ESA) for  $S_1 \rightarrow S_n$ transitions for NU-901. The ESA for NU-901 clearly differs from those of NU-1000 (Figure 5b, black) or H<sub>4</sub>TBAPy (Figure S11, black), which feature a sharp IA band near 740 nm (for NU-1000) or 700 nm (for H<sub>4</sub>TBAPy), respectively. Note that the TDDFT predicted  $S_1 \rightarrow S_n$  energy gap for  $H_4$ TBAPy is 1.701 eV (729 nm), whereas the corresponding

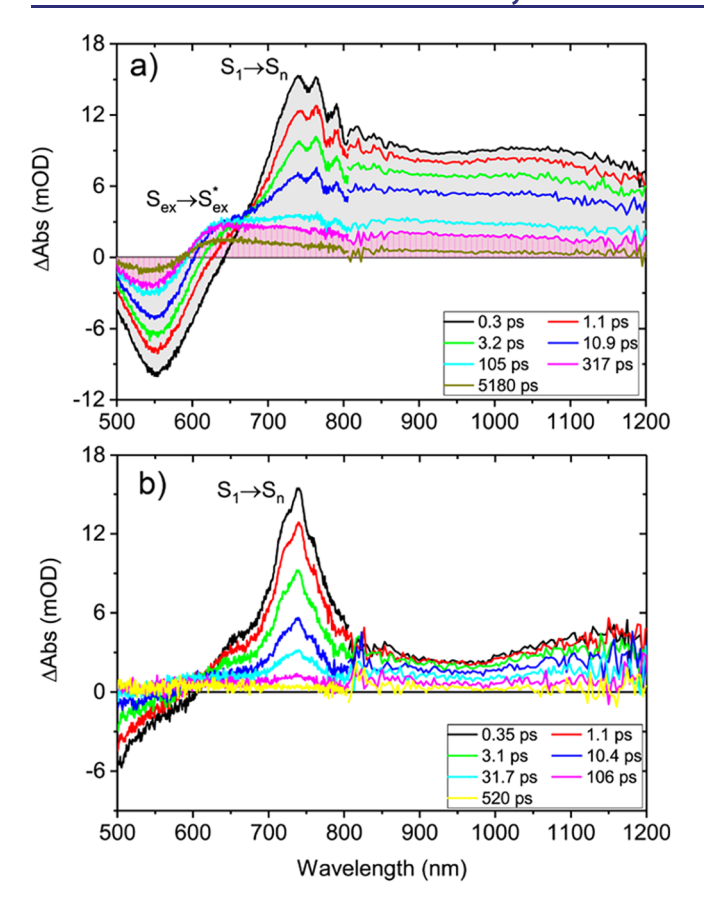


**Figure 5.** Representative femtosecond transient absorption spectra with  $\lambda_{\rm ex} = 400$  nm for (a) NU-901 and (b) NU-1000 deposited in a polystyrene matrix. Parallel pump/probe polarization. Excitation fluence =  $\sim 120~\mu {\rm J/cm^2}$ . Note that the structured spectral traces near 750–800 nm stem from the white-light generation using an 800 nm Ti:sapphire laser.

gaps for NU-1000t and NU-901z were computed to be 1.624 eV (763 nm) and 1.610 eV (770 nm), respectively. These computational data match exceedingly well with the trend observed in the fs-TA data and suggest that the interchromophoric excitonic interaction plays a crucial role in determining the energy gaps in their respective excited states. Furthermore, NU-901 renders spectral evolution (Figure 5a) with the emergence of a new IA band near 630 nm at  $t_{\rm delay} > 1$  ps, persisting beyond our instrument delay time limit ( $\sim$ 5 ns). This 630 nm IA band of NU-901, which spreads from 580 to 1100 nm, is absent in fs-TA spectral evolution in both NU-1000 and  $H_4$ TBAPy.

Global analysis for the fs-TA spectroscopic data for NU-901 determines that this broad 630 nm induced absorption band has a rise-time constant,  $\tau_{\rm rise}$  of 2.0 ps and a decay time constant,  $\tau_{\rm decay}$ , of 4.8 ns (Figure S10). The 4.8 ns time constant corresponds to the excimer emission lifetime of NU-901 reported in our previous report, <sup>12b</sup> and therefore, the 2.0 ps  $\tau_{\rm rise}$  corresponds to  $S_1 \rightarrow$  excimer formation. <sup>22</sup> Considering a close interchromophoric distance (9.52 Å) with a small pyrene–pyrene torsional angle (20°), the cofacial TBAPy linkers in the NU-901 structure are suitable for excimer-like complex formation (25% intensity). <sup>12b</sup> Although Douhal et al. reported a slow (~400–840 ps) excimer formation time in a naphthalene-based MOF by analyzing femtosecond emission transients, <sup>23</sup> our fs-TA spectra presented in Figure 5 thus underscore the first direct spectral observation of the excimer

formation in a MOF. Alternatively, in NU-1000, a longer interchromophoric distance and larger pyrene—pyrene torsional angle suppress the excimer formation, <sup>12b</sup> and thereby no significant excimer ESA can be seen in the fs-TA spectra (Figure 5b). The intensity of the NIR  $S_1 \rightarrow S_n$  ESA bands for NU-901 (Figure 5a) is comparable to their respective high  $S_1 \rightarrow S_0$  emissive oscillator strength. Such broad, intense ESA bands that extend into the NIR signify that these structures possess electronic states that are significantly delocalized in nature, corroborating with the TDDFT predictions (*vide supra*).

TDDFT-TDM analyses also suggest the existence of polar excited states with charge-transfer (CT) character defined by dominating off-diagonal and negligible diagonal densities (i.e., electron and hole reside in two different TBAPy units; denoted as CT<sub>1</sub>; Figures 6 and S5). The extent of the e—h separation in

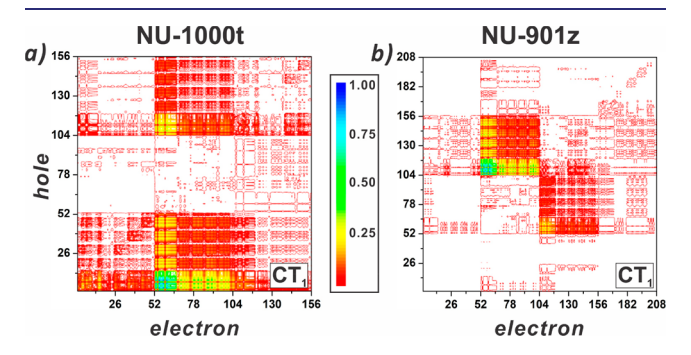


**Figure 6.** Contour plot of TDMs corresponding to spectroscopically relevant CT<sub>1</sub> excited states for model compounds NU-1000t and NU-901z (shown in Figure 3).

these CT states can go beyond two adjacent TBAPy units in the linear NU-901z; however, a longer separation will result in higher energy (thus denoted as  $CT_n$  in Figure 3, where n is the number of TBAPy units by which e—h separation occurred; Figure S5). Interestingly, depending on the framework topology, some of the polar excited states can have sizable oscillator strength for electronic transitions from the ground state. These optically allowed polar excited states in NU-1000t energetically reside close to the  $S_2$  state ( $CT_n$  states in the NU-901z model possess zero oscillator strength). Interestingly, the evolution of such polar excited states, as in the models, is without the involvement of any pyrene to Zr-oxo node LMCT species, rather solely of interchromophoric interactions.

To determine the possible role of these polar excited states in the emissive decay process, we examined transient fluorescence decays in various solvents. As shown in Figure 7, the transient fluorescence decay profiles for the NU-901 sample essentially remain unchanged in all the solvents except for the DMF. In contrast, the NU-1000 sample manifests solvent-dependent decay profiles. The corresponding lifetime data are summarized in Table SI-1 and are consistent with our previous report. 12b Considering the single-component fluorescence decay profiles for H<sub>4</sub>TBAPy,<sup>25</sup> showing little dependence on the solvent, our experimental data reveal that NU-1000 manifests a faster decay particularly in a more polar solvent such as acetonitrile. These data suggest that either the emissive states of NU-1000 have polar character and/or the solvent-responsive low-lying polar excited states play a key role in the excited-state dynamical process.

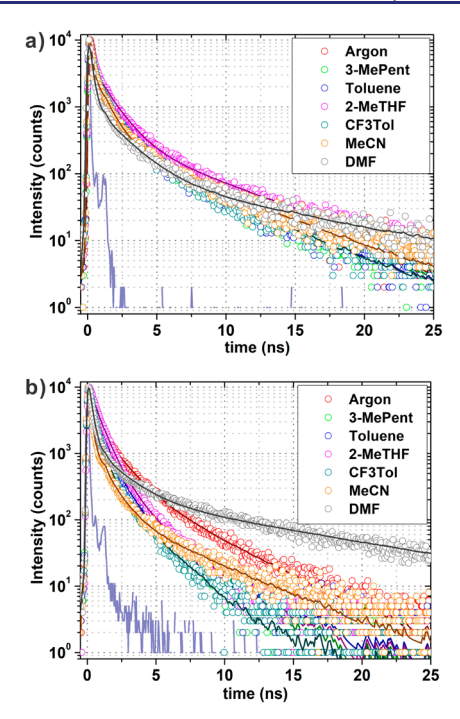


Figure 7. Transient emission decay profiles for (a) NU-901 ( $\lambda_{\text{probe}}$  = 520 nm) and (b) NU-1000 ( $\lambda_{\text{probe}} = 475 \text{ nm}$ ) collected in various solvents ( $\lambda_{ex}$  = 405 nm; the solid lines represent the reconvolution based fits, and the time constant outputs are summerized in Table SI-1).

Excitation-emission mapping spectra of these MOF samples, measured as a function of solvent polarity, provide crucial information on the transition energies to determine if the emissive state is polar in nature (Figure 8 and Figures S12

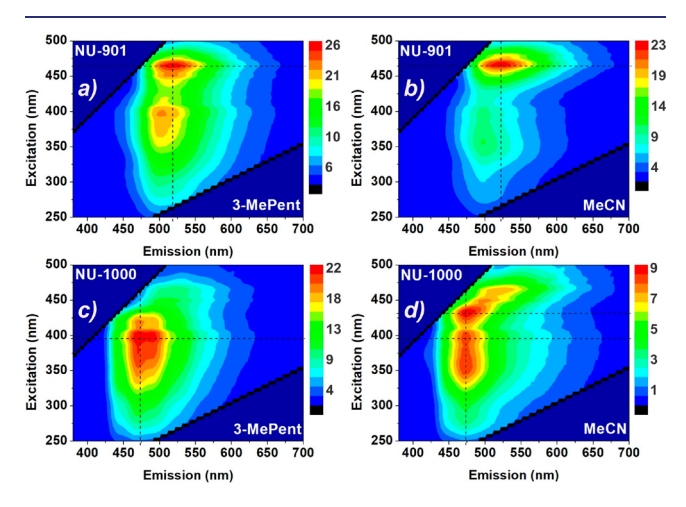


Figure 8. Excitation-emission mapping spectra recorded for (a,b) NU-901 and (c,d) NU-1000 suspended in 3-methyl pentane (a,c) and acetonitrile (b,d) solvents (experimental condition: RT; intensity is factored by  $10^{-4}$ ).

and S13). For NU-901 and NU-1000, the most intense peak appears at 520 nm ( $\lambda_{\rm ex}$  = 465 nm; Figure 8a,b) and 475 nm ( $\lambda_{\rm ex}$  = 395 and 425 nm; Figure 8c,d), <sup>12b</sup> respectively. For both samples, the corresponding emissive transition energies were found essentially unchanged with solvent polarity. 26 These data are consistent with the computational results confirming the nonpolar electronic structure of the respective emissive states

for both MOF samples. However, the relative contribution of the 395 and 425 nm excitation branches in NU-1000 appears to depend on the solvent, where the intensity of the 425 nm excitation branch ( $\lambda_{em}$  = 475 nm) becomes more pronounced in polar solvents, particularly those with a high acceptor number such as  $\alpha_1\alpha_2$  -trifluorotoluene (CF<sub>3</sub>Tol) and acetonitrile (MeCN).

Absolute fluorescence QY values can provide information regarding the extent of excited-state population that decay to the ground state via a nonradiative pathway. Data summarized in Figure 9 indicate that QY of NU-901 is less affected (QY =

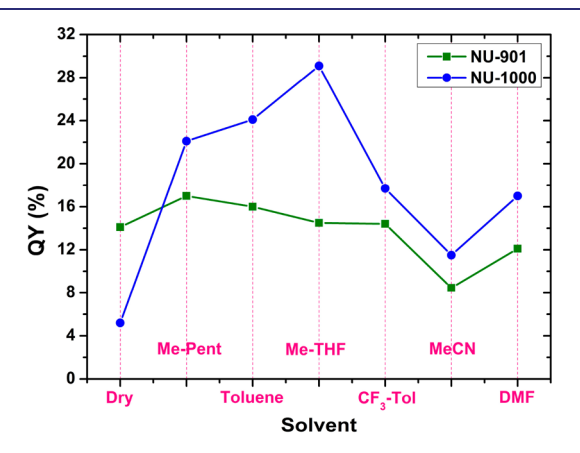


Figure 9. Solvent-dependent quantum yields from the most intense emission peaks recorded for samples NU-901 (520 nm) and NU-1000 (475 nm).

 $10 \pm 2\%$ ) by solvents except for MeCN. In comparison, NU-1000 shows a sizable variation on solvent: a dry NU-1000 sample renders the lowest QY value, which is enhanced in low dielectric media and finally diminished with an increase in solvent polarity (MeCN being the lowest). As all the experimental setup employed for these solid samples guaranteed that only a given set of chromophore linkers in the solid MOF samples are subjected to a constant and prolonged exposure to the excitation beam, solvation should facilitate local heat dissipation pathways to provide higher QY. Thus, in general, a solvent that interacts strongly (quantified with solvent dispersity) should provide a higher QY. However, no direct correlation of the observed trend in the QY values for the NU-1000 sample can be made with one particular solvent parameter (see Table SI-2 for various solvation parameters). Solvent dispersity may only explain an enhancement of the QY value from a dry sample to toluene to 2-MeTHF but fails to explain the QY trend recorded in the rest of the solvents as toluene, 2-MeTHF, CF<sub>3</sub>-Tol, and DMF possess a comparable dispersity parameter ( $\delta_D$ ; Table SI-2). However, considering the solvent acceptor number (AN) along with the dispersity constants ( $\delta_{\rm D}$ ), we can qualitatively explain the observed trend in QY values recorded for NU-1000.

It should be noted that, although the S<sub>1</sub> state is the lowest singlet state in the free H<sub>4</sub>TBAPy linker, the scenario is different in the chromophore assembly in a framework. Computational data indicate the existence of an optically forbidden dark excitonic state (zero-negligible  $S_0 \rightarrow D_1$ oscillator strength); the most significant are those that lie below the optically active  $S_1$  states ( $\sim 0.03-0.1$  eV; Figure 3 shown as  $D_1$  states). Figure 10 highlights the TDMs for the  $D_1$ states for two model compounds and are reminiscent of the

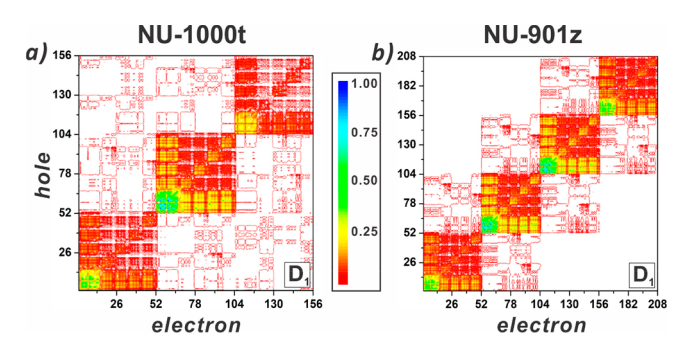


Figure 10. Contour plot of TDMs corresponding to spectroscopically relevant D<sub>1</sub> excited states for NU-1000t and NU-901z model compounds.

TDMs for corresponding  $S_1$  states (Figure 4a,c). Due to a similar delocalization property, these D<sub>1</sub> states are expected to provide a major nonradiative excited-state decay channel. Our experimental data suggest that these MOF samples have ~65-80% reduction in their quantum efficiencies compared to that of the free H<sub>4</sub>TBAPy linker (~85%<sup>25</sup>).<sup>27</sup> Whereas a high chromophore concentration in these solid MOFs can be a plausible reason, their emission spectra (Figure S2) do not show any sign of shape change at their higher energy side, indicating no inner-filter effect. Given that solvation marginally improves the QY, other nonradiative decay channels must exist. Considering that exciton annihilation commences only at high excitation fluences, we infer that the existence of a dark state can be possible in these solid compositions.<sup>2</sup>

For NU-1000, solvents with a higher AN were found to reduce the QY possibly via the activation of a nonradiative decay pathway through the optically allowed polar excited states. As the energy levels of these polar excited states (Figure 3) are susceptible to solvent electronic properties (such as AN), their involvement in the excited-state decay process can be altered by the solvent. In contrast, for NU-901, all the polar excited states are optically forbidden and may not get involved in the respective excited-state dynamical processes.

### CONCLUSION

We have studied the excited-state properties in two chemically identical but topologically different tetraphenylpyrene (1,3,6,8tetrakis(p-benzoicacid)pyrene; H<sub>4</sub>TBAPy)-based Zr<sup>IV</sup> MOFs, NU-901 (scu) and NU-1000 (csq). These structures differ in the concentration and orientation of chromophoric linkers they house within their networks. The structural parameters play a key role in the interchromophoric interactions that manifest in unique excited states that exhibit distinct photophysical properties.

TDDFT computations on various small TBAPy model compounds predict the evolution of various distinct excited states whose electronic structures depend on the MOF topology. For example, analysis of respective transition density matrix suggests that the wave function of the optically allowed S<sub>1</sub> and S<sub>2</sub> states are delocalized over multiple TBAPy linkers with maximum exciton size of ~1.7 nm (about two TBAPy chromophores). Furthermore, computational results predict the evolution of polar excited states with an electronic structure possessing charge-transfer character, where the extent of interchromophoric interaction dictates whether these states are optically allowed. For example, the NU-1000 framework is predicted to possess optically allowed CT states, whereas NU-901 renders optically forbidden CT states.

Femtosecond transient absorption spectroscopic data of NU-901 clearly contrast those recorded for NU-1000 and the H<sub>4</sub>TBAPy linker. NU-901 displays TA spectral evolution featuring an instantaneous  $S_1 \rightarrow S_n$  induced absorption at around 750 nm that diminishes with the emergence of a broad (580-1100 nm) induced absorption originating from an excimer formation. In contrast, NU-1000 and the reference linker compound (H<sub>4</sub>TBAPy) lack such spectral evolution. Dynamical analysis of this unprecedented spectral evolution underscores that a short interchromophoric distance (9.52 Å) and a small pyrene-pyrene torsional angle (20°) in NU-901 facilitate a fast excimer formation ( $au_{rise}$  of 2.0 ps) that last for several nanoseconds ( $au_{decay}$  of 4.8 ns). Although our previous work reported the excimeric emission lifetime ( $\tau = 4.8 \text{ ns}$ ) for NU-901, 12b the formation time and the ESA feature of excimers in this structure were unknown. In this regard, this the first direct spectral observation of excimer formation and spectral feature in MOF.

Transient and steady-state fluorescence data collected as a function of solvent polarity provide insight into the electronic nature of the emissive state: excitation-emission transition energies were found to show little dependence on solvent, indicating a nonpolar nature of the emissive S<sub>1</sub> excitonic states in these MOF samples. However, solvent-dependent fluorescence decay profiles, as well as their corresponding quantum yields, clearly suggest that low-lying polar excitonic states may influence the excited-state population decay process in one MOF sample more than other. Furthermore, the high oscillator strength of the observed  $S_1 \rightarrow S_n$  transitions in these MOF samples can be a subject of future investigations considering that light-harvesting compositions require low band gap materials with a strong singlet manifold transitions ( $S_0 \rightarrow S_1$ ,  $S_1 \rightarrow S_0$ , and  $S_1 \rightarrow S_n$ ) that span broad spectral domains including the NIR region. The results presented here suggest that chromophore assembly in the MOF can be optimized to achieve low-lying excited states with an unusual degree of electronic delocalization or polar character, which may lead to a weakly bound exciton to boost exciton dissociation and subsequent charge career generation.

#### **ASSOCIATED CONTENT**

## **S** Supporting Information

The Supporting Information is available free of charge on the ACS Publications website at DOI: 10.1021/jacs.8b04980.

Experimental details, computational and spectroscopic data (PDF)

# AUTHOR INFORMATION

# **Corresponding Author**

\*pderia@siu.edu

ORCID ®

Jierui Yu: 0000-0001-8422-3583 JaeHong Park: 0000-0002-0509-3934 Garry Rumbles: 0000-0003-0776-1462 Pravas Deria: 0000-0001-7998-4492

# **Present Address**

<sup>¶</sup>Department of Chemistry, Simpson College, 701 North C Street, Indianola, IA 50125, USA.

#### **Author Contributions**

 $^{\perp}$ J.Y. and J.P. contributed equally.

#### **Notes**

The authors declare no competing financial interest.

#### ACKNOWLEDGMENTS

We thank SIUC for the startup support. P.D. acknowledges Ralph E. Powe Junior Faculty Enhancement Award, administered by ORAU. A.V.W. acknowledges a NSF-REU fellowship (NSF Grant DMR-1461255). J.P. acknowledges JSPS KAKENHI Grant-in-Aid for Research Activity Start-up Grant Number 17H06791. J.P. also acknowledges Unisoku Co., Ltd. and Dr. Tatsuo Nakagawa for their assistance on transient absorption spectroscopic measurements. The initial photophysical characterization data were funded by the Division of Chemical Sciences, Geosciences, and Biosciences, Office of Basic Energy Sciences, Solar Photochemistry program of the U.S. Department of Energy through Grant DE-AC36-08-GO28308 to the National Renewable Energy Laboratory.

# REFERENCES

- (1) (a) Haycock, R. A.; Yartsev, A.; Michelsen, U.; Sundström, V.; Hunter, C. A. Angew. Chem., Int. Ed. 2000, 39, 3616-3619. (b) Li, X.; Sinks, L. E.; Rybtchinski, B.; Wasielewski, M. R. J. Am. Chem. Soc. 2004, 126, 10810-10811. (c) Kelley, R. F.; Lee, S. J.; Wilson, T. M.; Nakamura, Y.; Tiede, D. M.; Osuka, A.; Hupp, J. T.; Wasielewski, M. R. J. Am. Chem. Soc. 2008, 130, 4277-4284. (d) Röger, C.; Miloslavina, Y.; Brunner, D.; Holzwarth, A. R.; Würthner, F. J. Am. Chem. Soc. 2008, 130, 5929-5939. (e) Wasielewski, M. R. Acc. Chem. Res. 2009, 42, 1910-1921. (f) Frischmann, P. D.; Mahata, K.; Würthner, F. Chem. Soc. Rev. 2013, 42, 1847-1870.
- (2) Tretiak, S.; Mukamel, S. Chem. Rev. 2002, 102, 3171-3212.
- (3) (a) Scholes, G. D.; Gould, I. R.; Cogdell, R. J.; Fleming, G. R. J. Phys. Chem. B 1999, 103, 2543-2553. (b) Scholes, G. D.; Fleming, G. R. J. Phys. Chem. B 2000, 104, 1854-1868. (c) Tretiak, S.; Middleton, C.; Chernyak, V.; Mukamel, S. J. Phys. Chem. B 2000, 104, 4519-4528. (d) Scholes, G. D.; Fleming, G. R.; Olaya-Castro, A.; van Grondelle, R. Nat. Chem. 2011, 3, 763-774.
- (4) (a) Kasha, M.; Rawls, H. R.; Ashraf El-Bayoumi, M. Pure Appl. Chem. 1965, 11, 371-392. (b) Barber, J.; Andersson, B. Nature 1994, 370, 31-34. (c) Kühlbrandt, W.; Wang, D. N.; Fujiyoshi, Y. Nature 1994, 367, 614-621. (d) Markovitsi, D.; Germain, A.; Millié, P.; Lécuyer, P.; Gallos, L. K.; Argyrakis, P.; Bengs, H.; Ringsdorf, H. J. Phys. Chem. 1995, 99, 1005-1017. (e) Duncan, T. V.; Susumu, K.; Sinks, L. E.; Therien, M. J. J. Am. Chem. Soc. 2006, 128, 9000-9001. (f) Sagara, Y.; Kato, T. Nat. Chem. 2009, 1, 605-610. (g) O'Sullivan, M. C.; Sprafke, J. K.; Kondratuk, D. V.; Rinfray, C.; Claridge, T. D. W.; Saywell, A.; Blunt, M. O.; O'Shea, J. N.; Beton, P. H.; Malfois, M.; Anderson, H. L. Nature 2011, 469, 72-75. (h) Yang, J.; Yoon, M.-C.; Yoo, H.; Kim, P.; Kim, D. Chem. Soc. Rev. 2012, 41, 4808-4826.
- (5) (a) Zhou, H.; Yang, L.; Price, S. C.; Knight, K. J.; You, W. Angew. Chem., Int. Ed. 2010, 49, 7992-7995. (b) Lin, L.-Y.; Chen, Y.-H.; Huang, Z.-Y.; Lin, H.-W.; Chou, S.-H.; Lin, F.; Chen, C.-W.; Liu, Y.-H.; Wong, K.-T. J. Am. Chem. Soc. 2011, 133, 15822-15825. (c) Lu, L. Y.; Yu, L. P. Adv. Mater. 2014, 26, 4413-4430.
- (6) (a) Yaghi, O. M.; O'Keeffe, M.; Ockwig, N. W.; Chae, H. K.; Eddaoudi, M.; Kim, J. Nature 2003, 423, 705-714. (b) Férey, G. Chem. Soc. Rev. 2008, 37, 191-214.
- (7) (a) Kent, C. A.; Mehl, B. P.; Ma, L.; Papanikolas, J. M.; Meyer, T. J.; Lin, W. J. Am. Chem. Soc. 2010, 132, 12767-12769. (b) Kent, C. A.; Liu, D.; Ma, L.; Papanikolas, J. M.; Meyer, T. J.; Lin, W. J. Am. Chem. Soc. 2011, 133, 12940-12943. (c) Shigematsu, A.; Yamada, T.; Kitagawa, H. J. Am. Chem. Soc. 2011, 133, 2034-2036. (d) Cui, Y.; Yue, Y.; Qian, G.; Chen, B. Chem. Rev. 2012, 112, 1126-1162. (e) Jeong, N. C.; Samanta, B.; Lee, C. Y.; Farha, O. K.; Hupp, J. T. J. Am. Chem. Soc. 2012, 134, 51-54. (f) Kreno, L. E.; Leong, K.; Farha, O. K.; Allendorf, M.; Van Duyne, R. P.; Hupp, J. T. Chem. Rev. 2012, 112, 1105-1125. (g) Wang, C.; Zhang, T.; Lin, W. Chem. Rev. 2012, 112, 1084-1104. (h) Kung, C.-W.; Wang, T. C.; Mondloch, J. E.;

- Fairen-Jimenez, D.; Gardner, D. M.; Bury, W.; Klingsporn, J. M.; Barnes, J. C.; Van Duyne, R.; Stoddart, J. F.; Wasielewski, M. R.; Farha, O. K.; Hupp, J. T. Chem. Mater. 2013, 25, 5012-5017. (i) So, M. C.; Jin, S.; Son, H.-J.; Wiederrecht, G. P.; Farha, O. K.; Hupp, J. T. J. Am. Chem. Soc. 2013, 135, 15698-15701. (j) Son, H.-J.; Jin, S.; Patwardhan, S.; Wezenberg, S. J.; Jeong, N. C.; So, M.; Wilmer, C. E.; Sarjeant, A. A.; Schatz, G. C.; Snurr, R. Q.; Farha, O. K.; Wiederrecht, G. P.; Hupp, J. T. J. Am. Chem. Soc. 2013, 135, 862-869.
- (8) (a) Lin, J.; Hu, X.; Zhang, P.; Van Rynbach, A.; Beratan, D. N.; Kent, C. A.; Mehl, B. P.; Papanikolas, J. M.; Meyer, T. J.; Lin, W.; Skourtis, S. S.; Constantinou, M. J. Phys. Chem. C 2013, 117, 22250-22259. (b) Maza, W. A.; Ahrenholtz, S. R.; Epley, C. C.; Day, C. S.; Morris, A. J. J. Phys. Chem. C 2014, 118, 14200-14210. (c) Williams, D. E.; Rietman, J. A.; Maier, J. M.; Tan, R.; Greytak, A. B.; Smith, M. D.; Krause, J. A.; Shustova, N. B. J. Am. Chem. Soc. 2014, 136, 11886-11889. (d) Goswami, S.; Ma, L.; Martinson, A. B. F.; Wasielewski, M. R.; Farha, O. K.; Hupp, J. T. ACS Appl. Mater. Interfaces 2016, 8, 30863-30870.
- (9) Liu, Y. H.; Zhao, J. B.; Li, Z. K.; Mu, C.; Ma, W.; Hu, H. W.; Jiang, K.; Lin, H. R.; Ade, H.; Yan, H. Nat. Commun. 2014, 5, 5293. (10) (a) Ajayaghosh, A. Chem. Soc. Rev. 2003, 32, 181-191. (b) Zhou, H.; Yang, L.; Stuart, A. C.; Price, S. C.; Liu, S.; You, W. Angew. Chem., Int. Ed. 2011, 50, 2995-299.
- (11) Schmitz, R. A.; Liddell, P. A.; Kodis, G.; Kenney, M. J.; Brennan, B. J.; Oster, N. V.; Moore, T. A.; Moore, A. L.; Gust, D. Phys. Chem. Chem. Phys. 2014, 16, 17569-17579.
- (12) (a) Deria, P.; Yu, J.; Balaraman, R. P.; Mashni, J.; White, S. N. Chem. Commun. 2016, 52, 13031-13034. (b) Deria, P.; Yu, J.; Smith, T.; Balaraman, R. P. J. Am. Chem. Soc. 2017, 139, 5973-5983.
- (13) Bai, Y.; Dou, Y.; Xie, L.-H.; Rutledge, W.; Li, J.-R.; Zhou, H.-C. Chem. Soc. Rev. 2016, 45, 2327-2367.
- (14) (a) Cavka, J. H.; Jakobsen, S.; Olsbye, U.; Guillou, N.; Lamberti, C.; Bordiga, S.; Lillerud, K. P. J. Am. Chem. Soc. 2008, 130, 13850-13851. (b) deKrafft, K. E.; Boyle, W. S.; Burk, L. M.; Zhou, O. Z.; Lin, W. J. Mater. Chem. 2012, 22, 18139-18144. (c) Feng, D.; Gu, Z.-Y.; Li, J.-R.; Jiang, H.-L.; Wei, Z.; Zhou, H.-C. Angew. Chem., Int. Ed. 2012, 51, 10307-10310. (d) Deria, P.; Mondloch, J. E.; Tylianakis, E.; Ghosh, P.; Bury, W.; Snurr, R. Q.; Hupp, J. T.; Farha, O. K. J. Am. Chem. Soc. 2013, 135, 16801-16804. (e) Jiang, H.-L.; Feng, D.; Wang, K.; Gu, Z.-Y.; Wei, Z.; Chen, Y.-P.; Zhou, H.-C. J. Am. Chem. Soc. 2013, 135, 13934-13938. (f) Mondloch, J. E.; Bury, W.; Fairen-Jimenez, D.; Kwon, S.; DeMarco, E. J.; Weston, M. H.; Sarjeant, A. A.; Nguyen, S. T.; Stair, P. C.; Snurr, R. Q.; Farha, O. K.; Hupp, J. T. J. Am. Chem. Soc. 2013, 135, 10294-10297. (g) Wu, H.; Yildirim, T.; Zhou, W. J. Phys. Chem. Lett. 2013, 4, 925-930. (h) Deria, P.; Bury, W.; Hupp, J. T.; Farha, O. K. Chem. Commun. 2014, 50, 1965-1968. (i) Kalidindi, S. B.; Nayak, S.; Briggs, M. E.; Jansat, S.; Katsoulidis, A. P.; Miller, G. J.; Warren, J. E.; Antypov, D.; Corà, F.; Slater, B.; Prestly, M. R.; Martí-Gastaldo, C.; Rosseinsky, M. J. Angew. Chem., Int. Ed. 2015, 54, 221. (j) Deria, P.; Chung, Y. G.; Snurr, R. Q.; Hupp, J. T.; Farha, O. K. Chem. Sci. 2015, 6, 5172-5176. (k) Deria, P.; Gómez-Gualdrón, D. A.; Bury, W.; Schaef, H. T.; Wang, T. C.; Thallapally, P. K.; Sarjeant, A. A.; Snurr, R. Q.; Hupp, J. T.; Farha, O. K. J. Am. Chem. Soc. 2015, 137, 13183-13190. (1) Wang, T. C.; Bury, W.; Gómez-Gualdrón, D. A.; Vermeulen, N. A.; Mondloch, J. E.; Deria, P.; Zhang, K.; Moghadam, P. Z.; Sarjeant, A. A.; Snurr, R. Q.; Stoddart, J. F.; Hupp, J. T.; Farha, O. K. J. Am. Chem. Soc. 2015, 137, 3585-3591. (m) Deria, P.; Gómez-Gualdrón, D. A.; Hod, I.; Snurr, R. Q.; Hupp, J. T.; Farha, O. K. J. Am. Chem. Soc. 2016, 138, 14449-14457.
- (15) (a) Hod, I.; Bury, W.; Gardner, D. M.; Deria, P.; Roznyatovskiy, V.; Wasielewski, M. R.; Farha, O. K.; Hupp, J. T. J. Phys. Chem. Lett. 2015, 6, 586-591. (b) McGonigal, P. R.; Deria, P.; Hod, I.; Moghadam, P. Z.; Avestro, A.-J.; Horwitz, N. E.; Gibbs-Hall, I. C.; Blackburn, A. K.; Chen, D.; Botros, Y. Y.; Wasielewski, M. R.; Snurr, R. Q.; Hupp, J. T.; Farha, O. K.; Stoddart, J. F. Proc. Natl. Acad. Sci. U. S. A. 2015, 112, 11161-11168.
- (16) (a) Park, J.; Reid, O. G.; Rumbles, G. J. Phys. Chem. B 2015, 119, 7729-7739. (b) Ortiz, M.; Cho, S.; Niklas, J.; Kim, S.;

Poluektov, O. G.; Zhang, W.; Rumbles, G.; Park, J. J. Am. Chem. Soc. **2017**, 139, 4286–4289.

- (17) Shi, T.; Wang, P. J. Mol. Graphics Model. 2016, 70, 305–314. (18) (a) Hendrickx, K.; Vanpoucke, D. E. P.; Leus, K.; Lejaeghere, K.; Van Yperen-De Deyne, A.; Van Speybroeck, V.; Van Der Voort, P.; Hemelsoet, K. Inorg. Chem. 2015, 54, 10701–10710. (b) Nasalevich, M. A.; Hendon, C. H.; Santaclara, J. G.; Svane, K.; van der Linden, B.; Veber, S. L.; Fedin, M. V.; Houtepen, A. J.; van der Veen, M. A.; Kapteijn, F.; Walsh, A.; Gascon, J. Sci. Rep. 2016, 6, 23676. (c) De Vos, A.; Hendrickx, K.; Van Der Voort, P.; Van Speybroeck, V.; Lejaeghere, K. Chem. Mater. 2017, 29, 3006–3019. (d) Wu, X.-P.; Gagliardi, L.; Truhlar, D. G. J. Am. Chem. Soc. 2018, 140, 7904–7912. (19) Yanai, T.; Tew, D. P.; Handy, N. C. Chem. Phys. Lett. 2004, 393, 51–57.
- (20) Mukamel, S.; Tretiak, S.; Wagersreiter, T.; Chernyak, V. Science 1997, 277, 781–787.
- (21) (a) Tretiak, S.; Chernyak, V.; Mukamel, S. *Phys. Rev. Lett.* **1996**, 77, 4656–4659. (b) Tretiak, S. *Nano Lett.* **2007**, 7, 2201–2206.
- (22) Additional slower  $S_1$  state decay components (43 ps and 1.0 ns) are also determined; these may correspond to singlet-singlet annihilation and localized  $S_1$  state decay.
- (23) (a) Gutierrez, M.; Sanchez, F.; Douhal, A. Phys. Chem. Chem. Phys. **2016**, 18, 5112-5120. (b) Gutiérrez, M.; Sánchez, F.; Douhal, A. Chem. Eur. J. **2016**, 22, 13072-13082.
- (24) For example, oscillator strengths computed for NU-901 models are zero, whereas the polar excited state of the NU-1000t possesses significant optical allowance.
- (25) El-Assaad, T. H.; Auer, M.; Castañeda, R.; Hallal, K. M.; Jradi, F. M.; Mosca, L.; Khnayzer, R. S.; Patra, D.; Timofeeva, T. V.; Brédas, J.-L.; List-Kratochvil, E. J. W.; Wex, B.; Kaafarani, B. R. J. Mater. Chem. C 2016, 4, 3041–3058.
- (26) Note that NU-1000 exerts a smaller red shift relative to NU-901 due to a longer center-to-center distance of ~11 Å and a relaxed TBAPy conformation defined by larger pyrene—pyrene and pyrene—phenyl torsional angles (60 and 50°). The TBAPy linkers adopt a strained conformation in NU-901 leading to a large red-shifted spectra (465/520 nm ex/em); thus, a solvent that exerts a strong interaction with the NU-901 framework can facilitate to adopt a "relaxed" NU-1000-like conformation. Indeed, the excitation—emission mapping spectra (Figures S12 and S13) as well as the fluorescence decay times of NU-901 in DMF (Table SI-1) are comparable to that of NU-1000 in DMF solvent. Thus, we infer that the weak peaks at 395/505 nm (ex/em) stem from the "relaxed" surface-bound TBAPy linkers.
- (27) A small  $S_1$ – $D_1$  energy gap can be expected to quench the emission to near completeness. Note that these TDDFT computations are based on the ground-state geometry. Thus, computation on an optimized excited-state geometry may provide a better picture. Nevertheless, such small gaps are also known in rigid carbon-based systems like single-walled carbon nanotubes (see ref 21b).
- (28) This finding is further supported by our fs-TA data, which clearly register disparity of decay dynamics between the  $S_1 \rightarrow S_n$  ESA peak and  $S_1 \rightarrow S_0$  stimulated emission peak, indicating a quick dissipation of significant amount of the  $S_1$  population.